ELSEVIER

International Journal of Heat and Fluid Flow 22 (2001) 30–38

International Journal of HEAT AND FLUID FLOW

www.elsevier.com/locate/ijhff

A new DNS algorithm for rotating homogeneous decaying turbulence

Y. Morinishi *, K. Nakabayashi, S.Q. Ren

Department of Mechanical Engineering, Nagoya Institute of Technology, Gokiso-cho, Showa-ku, Nagoya 466-8555, Japan

Received 29 February 2000; accepted 7 July 2000

Abstract

A new algorithm for simulating homogeneous decaying turbulence in an incompressible fluid subjected to uniform system rotation has been proposed. The integral factor technique has been extended to the Coriolis term. Since the Coriolis term is integrated analytically in the algorithm, the time increment is not restricted by the system rotation. It is verified that the new algorithm is effective at strong rotation. With this new algorithm, DNS of the homogeneous decaying turbulence is carried out to investigate the effects of the system rotation on the turbulence. The DNS results show that the system rotation inhibits the decay of the kinetic energy. The rotation induces an anisotropic distribution of the kinetic energy between the pole and the equator in wave space and elongates the vortical structure along the rotation axis in physical space. However, this rotation effect is only apparent at moderate rotation. © 2001 Elsevier Science Inc. All rights reserved.

Keywords: Numerical analysis; Stability condition; Turbulence; Direct numerical simulation; System rotation

1. Introduction

Direct numerical simulation (DNS) of the Navier–Stokes equation has been proved to be a powerful tool for turbulence analysis. DNS of fundamental turbulent flow, such as homogeneous decaying turbulence, the homogeneous shear turbulence and the wall-bounded planar turbulence, shows that it is a useful tool for turbulence structure analysis and turbulence modeling (Moin and Mahesh, 1998). With the development of computers, a number of fundamental turbulent flow fields can be calculated by DNS within the low-Reynolds number region. DNS has also been used to simulate rotating turbulence, an important type of fundamental turbulence field. Up to now, rotating decaying turbulence (e.g. Mansour et al. 1992; Teissedre and Dang, 1987), rotating turbulent Poiseuille flow (Tafti and Vanka, 1991; Yang and Kim, 1991; Kristoffersen and Anderson, 1993; Lamballais et al., 1996) and rotating turbulent plane Couette flow (Bech et al., 1995) have been calculated by DNS. The Navier–Stokes (N–S) equation of a rotating system has the Coriolis term, which can be expressed as the curl of the rotation vector $\boldsymbol{\Omega}$ and the velocity vector $\boldsymbol{u}$. Conventionally, the Coriolis term is usually integrated by an explicit time marching method in the same manner as a nonlinear term. However, the explicit method only allows a very small time increment for solving N–S equations with the Coriolis term. Hence, DNS of a rotating turbulence needs more CPU time than that without the Coriolis term. Furthermore, using an explicit method to solve the N–S equations with the Coriolis term will introduce a large diffusion error into the solution, and the reliability of the solution becomes poor. Hence, DNS of rotating turbulence has been limited to weak rotation so far.

In this paper, we first present the basic equations for rotating turbulence and discuss the numerical stability of a number of time marching methods. Then, a DNS algorithm for rotating decaying turbulence is proposed to integrate the Coriolis term analytically over time. With this DNS algorithm, there is no diffusion error and no limit to the time increment due to the Coriolis term. The pseudo-spectral method is adopted as the space differential scheme in this paper. By comparing the conventional algorithm for the Coriolis term with the present one, the validity of this DNS algorithm is verified. Finally, with this DNS algorithm, the influences of the system rotation on the turbulence statistics, the distribution of the energy spectrum and the turbulence structure are investigated with DNS of an initially isotropic rotating decaying turbulence.

2. Formulation and numerical stability

2.1. Basic equations

We consider an incompressible fluid flow subjected to uniform solid-body rotation at a rate Ω around the x_3-axis, without the mean velocity. The N–S and the continuity equations in this case are

$$\frac{\partial u_i}{\partial t}+\frac{\partial u_i u_j}{\partial x_j}=-\frac{\partial p}{\partial x_i}+\nu\frac{\partial^2 u_i}{\partial x_j\partial x_j}-2\Omega\varepsilon_{i3l}u_l, \tag{1}$$

* Corresponding author.
E-mail address: morinisi@cfd.mech.nitech.ac.jp (Y. Morinishi).

PII: S0142-727X(00)00067-9

Notation

$\boldsymbol{A}$	matrix, Eq. (7)
$\boldsymbol{D}$	$\boldsymbol{Q}^{-1}\boldsymbol{A}\boldsymbol{Q}$
D_ε	destruction term in Eq. (16)
$\boldsymbol{E}$	unit matrix in Eqs. (6) and (9)
E	energy spectrum
F	flatness factor of velocity gradient
I	complex unit, $(-1)^{1/2}$
K	kinetic energy
$\boldsymbol{k}$	wave number vector
k_p	wave number at which the energy spectrum takes a peak value
$L_{ij,k}$	integral lengthscale, Eq. (19)
$L_{33,3}$	longitudinal integral lengthscale
$L_{11,3}+L_{22,3}$	transverse integral lengthscale
L^*	$(L_{11,3}+L_{22,3})/L_{33,3}$
$\hat{\boldsymbol{M}}$	RHS of Eq. (6)
$\hat{\boldsymbol{N}}$	RHS of Eq. (9)
$\boldsymbol{n}^k$	unit vector along the direction axis x_k
$p, \hat{p}$	pressure
P_{im}	projection operator, $\delta_{im}-k_ik_m/k^2$
P_ε	production term in Eq. (16)
q_0	initial kinetic energy at $t=0$
$\boldsymbol{Q}$	matrix, Eq. (8.1)
$\boldsymbol{Q}^{-1}$	matrix, Eq. (8.2)
$\boldsymbol{r}$	vector of position
Re_t	turbulence Reynolds number, $(K^2/(v\varepsilon))$
Re_λ	Taylor microscale Reynolds number, $(K^{1/2}\lambda/v)$
Ro^L	macro Rossby number, $(u'/(2\Omega L_{33,3}))$
S	skewness factor of velocity gradient
t	time
t_0	initial time for DNS
Δt	time increment
u'	r.m.s. velocity
$\boldsymbol{u}, \hat{\boldsymbol{u}}$	velocity vector
$\hat{\boldsymbol{v}}$	$\boldsymbol{Q}^{-1}\hat{\boldsymbol{u}}$
$\boldsymbol{x}$	independent variable in Cartesian coordinate

Greeks

$\boldsymbol{\Omega}$	angular velocity of system rotation
v	kinetic viscosity
ε	dissipation rate of turbulence energy
θ	angle between $\boldsymbol{\Omega}$ and $\boldsymbol{k}$
λ	eigenvalue or Taylor microscale
λ^R	real part of the eigenvalue λ
λ^I	imaginary part of the eigenvalue λ

Subscripts

0	value at t_0
1, 2, 3	component of vector or direction of axis
i, j, k, l, m	component of vector or direction of axis

$$\frac{\partial u_i}{\partial x_i}=0. \tag{2}$$

The third term on the right-hand side (RHS) of Eq. (1) is the Coriolis term. The centrifugal acceleration $\boldsymbol{\Omega}\times(\boldsymbol{\Omega}\times\boldsymbol{r})$ is, as usual, included in the pressure. Using the Fourier Galerkin method (Canuto et al., 1987) to Eqs. (1) and (2), we obtain

$$\left(\frac{\mathrm{d}}{\mathrm{d}t}+vk^2\right)\hat{u}_i=-Ik_i\hat{p}-Ik_j\widehat{u_ju_i}-2\Omega\varepsilon_{i3j}\hat{u}_j, \tag{3}$$

$$Ik_i\hat{u}_i=0. \tag{4}$$

A caret ˆ denotes the Fourier transform. The pressure term in Eq. (3) can be removed by using the solenoidal condition Eq. (4). This operation reforms Eq. (3) to,

$$\left(\frac{\mathrm{d}}{\mathrm{d}t}+vk^2\right)\hat{u}_i=P_{im}(\boldsymbol{k})(-Ik_j\widehat{u_ju_m}-2\Omega\varepsilon_{m3j}\hat{u}_j). \tag{5}$$

Here $P_{im}(\boldsymbol{k})=\delta_{im}-k_ik_m/k^2$ is the solenoidal projection operator. The first and the second terms on the right-hand side correspond to the nonlinear and the Coriolis terms, respectively. The following discussion and simulation are based on this equation and its alteration.

2.2. Diagonalization

To analyze the numerical stability of the basic equation and then to propose a suitable DNS algorithm for rotating turbulence, we first diagonalize the basic equation (5). Using Eq. (4) to reformulate the Coriolis term, we can re-write Eq. (5) as the following equation:

$$\left[\left(\frac{\mathrm{d}}{\mathrm{d}t}+vk^2\right)\boldsymbol{E}+\frac{2\Omega k_3}{k^2}\boldsymbol{A}\right]\hat{\boldsymbol{u}}=\hat{\boldsymbol{M}}, \tag{6}$$

where $\boldsymbol{E}$ is the unit matrix, and vectors $\hat{\boldsymbol{u}}$ and $\hat{\boldsymbol{M}}$ are defined as

$$\hat{\boldsymbol{u}}=[\hat{u}_1,\hat{u}_2,\hat{u}_3]^\mathrm{T},\quad \hat{\boldsymbol{M}}=[\hat{M}_1,\hat{M}_2,\hat{M}_3]^\mathrm{T},\quad \hat{M}_i=-Ik_jP_{im}(\boldsymbol{k})\widehat{u_ju_m}.$$

In addition, the matrix $\boldsymbol{A}$ is defined as

$$\boldsymbol{A}=\begin{bmatrix}0 & -k_3 & +k_2\\ +k_3 & 0 & -k_1\\ -k_2 & +k_1 & 0\end{bmatrix}. \tag{7}$$

Solving the characteristic equation of the matrix $\boldsymbol{A}$, one obtains the eigenvalues $\lambda_1=+Ik$, $\lambda_2=-Ik$, and $\lambda_3=0$. The mode matrices corresponding to the eigenvalues of the matrix $\boldsymbol{A}$ take the following forms:

$$\boldsymbol{Q}=\frac{1}{[2k^2(k_2^2+k_3^2)]^{1/2}}\times\begin{bmatrix}(k_2^2+k_3^2) & (k_2^2+k_3^2) & [2k_1^2(k_2^2+k_3^2)]^{1/2}\\ (-k_1k_2-Ikk_3) & (-k_1k_2+Ikk_3) & [2k_2^2(k_2^2+k_3^2)]^{1/2}\\ (-k_1k_3+Ikk_2) & (-k_1k_3-Ikk_2) & [2k_3^2(k_2^2+k_3^2)]^{1/2}\end{bmatrix}, \tag{8.1}$$

$$\boldsymbol{Q}^{-1}=\frac{1}{[2k^2(k_2^2+k_3^2)]^{1/2}}\times\begin{bmatrix}(k_2^2+k_3^2) & (-k_1k_2+Ikk_3) & (-k_1k_3-Ikk_2)\\ (k_2^2+k_3^2) & (-k_1k_2-Ikk_3) & (-k_1k_3+Ikk_2)\\ [2k_1^2(k_2^2+k_3^2)]^{1/2} & [2k_2^2(k_2^2+k_3^2)]^{1/2} & [2k_3^2(k_2^2+k_3^2)]^{1/2}\end{bmatrix}. \tag{8.2}$$

The orthogonal vectors corresponding to the first and the second rows of $\boldsymbol{Q}^{-1}$, respectively, are just the basis vectors (multiply by a factor $1/2^{1/2}$) of the so-called 'complex helical waves decomposition' (Cambon and Jacquin, 1989; Waleffe, 1992; Lesieur, 1997). Using $\boldsymbol{Q}$ and $\boldsymbol{Q}^{-1}$, Eq. (6) can be brought in the following diagonal form:

$$\left[\left(\frac{\mathrm{d}}{\mathrm{d}t}+vk^2\right)\boldsymbol{E}+\frac{2\boldsymbol{\Omega}k_3}{k^2}\boldsymbol{D}\right]\hat{\boldsymbol{v}}=\hat{\boldsymbol{N}}, \tag{9}$$

with $\hat{v} = \boldsymbol{Q}^{-1}\hat{u}$, $\hat{N} = \boldsymbol{Q}^{-1}\hat{M}$ and

$$\boldsymbol{D} = \boldsymbol{Q}^{-1}\boldsymbol{A}\boldsymbol{Q} = \begin{bmatrix} \lambda_1 & 0 & 0 \\ 0 & \lambda_2 & 0 \\ 0 & 0 & \lambda_3 \end{bmatrix} = \begin{bmatrix} +Ik & 0 & 0 \\ 0 & -Ik & 0 \\ 0 & 0 & 0 \end{bmatrix}.$$

Therefore, the Coriolis term is diagonalized through this transformation.

2.3. Absolute stability condition

It is noted that the numerical stability of the time marching method of Eq. (5) is equivalent to that of Eq. (9). The stability of the time marching method about the linear term Eq. (9) can be estimated by investigating the following characteristic equation:

$$\frac{\mathrm{d}\phi}{\mathrm{d}t} = \lambda\phi, \quad \lambda = \lambda^{\mathrm{R}} + I\lambda^{\mathrm{I}}. \tag{10}$$

The analytical solution of Eq. (10) is $\phi(t) = \phi(0)\mathrm{e}^{\lambda t}$. In accordance with this equation, the absolute stability conditions for various time marching methods were investigated in detail (e.g. Gear, 1971; Canuto et al., 1987).

Table 1 summarizes the absolute stability regions of a number of time marching methods corresponding to real and imaginary parts of the eigenvalue of Eq. (10). In Table 1, AB1–AB4 refer to first- to fourth-order Adams–Bashforth (AB) type explicit time marching methods, respectively, and AM1–AM4 refer to first- to fourth-order Adams–Moulton (AM) type implicit time marching methods. RK2, RK3 and RK4 are second-, third- and fourth-order Runge–Kutta type explicit marching methods. In particular, AB1 and AM1 are called the explicit and implicit Euler methods, respectively, and AM2 is called the Crank–Nicolson method. The absolute stability conditions for the viscous and Coriolis terms of Eq. (9) can be obtained by assuming that $\lambda^{\mathrm{R}} = -\nu k^2$ and $\lambda^{\mathrm{I}} = \pm 2\Omega k_3/k$. Then, corresponding to the real and the imaginary parts of λ, respectively, one knows that the most strict limit takes place at $k = k_{\max}$ and $k_3 = k$. Hence, we will only discuss the case of $\lambda^{\mathrm{R}} = -\nu k_{\max}^2$ or $\lambda^{\mathrm{I}} = \pm 2\Omega$.

First we discuss the numerical stability of the time marching method for the viscous terms corresponding to the real part in Table 1. It shows that one can always find a certain time increment for each type of time marching method, which makes the numerical calculation absolutely stable. However, when AB or RK type time marching method is adopted, the time increment has to be set very small [$\Delta t \leqslant \mathrm{O}(1/\nu k_{\max}^2)$]. As shown in Table 1, there also exists a limit to the time increment for the implicit methods not lower than the third-order as well. AM1 and AM2 are stable time marching methods with a stability not dependent on the value of Δt. In fact, AM2 is the popular time marching method for the viscous term.

Table 1
Absolute stability regions

	Real part	Imaginary part
AB1	$0 \leqslant -\lambda^{\mathrm{R}}\Delta t \leqslant 2$	Unstable ($\lambda^{\mathrm{I}} \neq 0$)
AB2	$0 \leqslant -\lambda^{\mathrm{R}}\Delta t \leqslant 1$	Unstable ($\lambda^{\mathrm{I}} \neq 0$)
AB3	$0 \leqslant -\lambda^{\mathrm{R}}\Delta t \leqslant 0.545$	$0 \leqslant \lvert\lambda^{\mathrm{I}}\Delta t\rvert \leqslant 0.723$
AB4	$0 \leqslant -\lambda^{\mathrm{R}}\Delta t \leqslant 0.3$	$0 \leqslant \lvert\lambda^{\mathrm{I}}\Delta t\rvert \leqslant 0.430$
AM1	$0 \leqslant \lambda^{\mathrm{R}}\Delta t, 2 \leqslant \lambda^{\mathrm{R}}\Delta t$	$0 \leqslant \lvert\lambda^{\mathrm{I}}\Delta t\rvert$
AM2	$0 \leqslant -\lambda^{\mathrm{R}}\Delta t$	$0 \leqslant \lvert\lambda^{\mathrm{I}}\Delta t\rvert$
AM3	$0 \leqslant -\lambda^{\mathrm{R}}\Delta t \leqslant 6$	Unstable ($\lambda^{\mathrm{I}} \neq 0$)
AM4	$0 \leqslant -\lambda^{\mathrm{R}}\Delta t \leqslant 3$	Unstable ($\lambda^{\mathrm{I}} \neq 0$)
RK2	$0 \leqslant -\lambda^{\mathrm{R}}\Delta t \leqslant 2$	Unstable ($\lambda^{\mathrm{I}} \neq 0$)
RK3	$0 \leqslant -\lambda^{\mathrm{R}}\Delta t \leqslant 2.51$	$0 \leqslant \lvert\lambda^{\mathrm{I}}\Delta t\rvert \leqslant 1.73$
RK4	$0 \leqslant -\lambda^{\mathrm{R}}\Delta t \leqslant 2.79$	$0 \leqslant \lvert\lambda^{\mathrm{I}}\Delta t\rvert \leqslant 2.83$

Then, we discuss the numerical stability of the time marching methods for the Coriolis term corresponding to the imaginary part in Table 1. If $\Omega \neq 0$, i.e. $\lambda^{\mathrm{I}} \neq 0$, all the explicit methods lower than second-order (AB1, AB2, RK2) and all the implicit methods higher than third-order (AM3, AM4) in Table 1 are unstable. The Coriolis term in Eq. (5) has not been diagonalized, and it is usually solved by the explicit time marching method. It is necessary to choose a time marching method with an accuracy not lower than third-order when the Coriolis term is integrated by an explicit method. With such a method, the limit of the time increment is inversely proportional to the value of Ω, and it becomes very severe at a high rotation rate. AB2 has also been chosen for the Coriolis term in some of the literature (e.g. Hossain, 1994). Hossain (1994) denoted a fast increase of kinetic energy when the rotation is turned on, and it contrasts with the current knowledge of rotating turbulence evidently (Jacquin et al. 1990; Cambon et al. 1997).

The above stability analysis is made in wave space and based on the diagonalized equation (9). In physical space, one can evaluate the stability of the Coriolis term in the same way. Assuming $i = 1, 2$ in Eq. (1), the equations with only the time and the Coriolis terms are

$$\frac{\mathrm{d}u_1}{\mathrm{d}t} = +2\Omega u_2, \tag{11.1}$$

$$\frac{\mathrm{d}u_2}{\mathrm{d}t} = -2\Omega u_1. \tag{11.2}$$

If one defines $\phi = u_1 + Iu_2$, the system of differential equations above becomes

$$\frac{\mathrm{d}\phi}{\mathrm{d}t} = -I2\Omega\phi. \tag{12}$$

Comparing this equation with Eq. (10) and referring to Table 1, obviously, one can analyze the numerical stability for various time marching methods in physical space with the same procedure as that in wave space.

3. DNS algorithm for rotating turbulence

3.1. Integral factor technique

Rogallo (1981) proposed an integral factor technique, which integrates the viscous term analytically. By introducing the integral factor $\mathrm{e}^{\nu k^2 t}$ into Eq. (5) and reforming this equation, we find

$$\frac{\mathrm{d}}{\mathrm{d}t}\left(\mathrm{e}^{\nu k^2 t}\hat{u}_i\right) = \mathrm{e}^{\nu k^2 t}P_{im}(\boldsymbol{k})\Big(-Ik_j\widehat{u_j u_m} - 2\Omega\varepsilon_{m3j}\hat{u}_j\Big). \tag{13}$$

With the integral factor technique, $\mathrm{e}^{\nu k^2 t}\hat{u}_i$ becomes a new variable. The advantages of this technique are that there is no limit to the time increment and no numerical error from the viscous term. Hence, it can be argued that the integral factor technique for the viscous term is more useful than AM1 or AM2 for solving Eq. (5). However, the time increment in a rotating system is still limited to the absolute stability conditions for the nonlinear and the Coriolis terms even with this integral factor technique. Here we denote the DNS algorithm for Eq. (13) with RK4 for the nonlinear and the Coriolis terms as "standard" in this paper. From Table 1, the limit of the time increment of the standard algorithm from the Coriolis term is $\Delta t \leqslant 2.83/(2\Omega)$.

3.2. Integral factor technique for the Coriolis term

The analysis above shows that, although the Coriolis and the viscous terms are both linear, the former is not integrated analytically with the standard algorithm, and that it still limits the time increment. In this paper, we propose a new integral factor technique on the basis of Eq. (9), so that the Coriolis and the viscous terms can both be integrated analytically. With this technique, the time increment Δt will not be limited to the rotation rate Ω.

Introducing a rotating integral factor $e^{(\nu k^2 \pm I2\Omega k_3/k)t}$ into Eq. (9), we find

$$\frac{\mathrm{d}}{\mathrm{d}t}\left[\exp\left\{\left(\nu k^2 + I\frac{2\Omega k_3}{k}\right)t\right\}\hat{v}_1\right] = \exp\left\{\left(\nu k^2 + I\frac{2\Omega k_3}{k}\right)t\right\}\hat{N}_1, \tag{14.1}$$

$$\frac{\mathrm{d}}{\mathrm{d}t}\left[\exp\left\{\left(\nu k^2 - I\frac{2\Omega k_3}{k}\right)t\right\}\hat{v}_2\right] = \exp\left\{\left(\nu k^2 - I\frac{2\Omega k_3}{k}\right)t\right\}\hat{N}_2. \tag{14.2}$$

If one takes $\exp\{(\nu k^2 + I2\Omega k_3/k)t\}\hat{v}_1$ and $\exp\{(\nu k^2 - I2\Omega k_3/k)t\}\hat{v}_2$ as new variables, Eqs. (14.1) and (14.2) are integrated with RK4 in time. With this new technique, only the stability condition for the nonlinear term will restrict the time increment. The transfers $\hat{\boldsymbol{v}} = \boldsymbol{Q}^{-1}\hat{\boldsymbol{u}}$ and $\hat{\boldsymbol{N}} = \boldsymbol{Q}^{-1}\hat{\boldsymbol{M}}$ are used in this algorithm. In addition, we find that $\hat{v}_3 = \hat{N}_3 = 0$ according to the definition of $\boldsymbol{Q}^{-1}$ and the solenoidal condition. We denote this new DNS algorithm for Eqs. (14.1) and (14.2) as "present". In the process of reviewing this paper, we found that Yeung and Zhou (1998) and Smith and Waleffe (1999) also developed a similar technique in simulating forced rotating turbulence, but no detailed scheme and no numerical stability analysis are presented in their papers.

3.3. Validation

In order to verify the algorithm mentioned above, we use it to calculate an initially isotropic homogeneous decaying turbulence subjected to system rotation and compare the results with those of the standard algorithm. The computational region and the spectral mode number are set as 2π and 32, respectively. The kinetic viscosity and the rotation rate are $\nu = 0.01$ m^2/s and $\Omega = 100$ rad/s, respectively. The time increment is varied from 0.0002 to 0.02 s. A velocity field with a random phase in wave space is produced, and the initial field is obtained by pre-computing this field to time t_0 with $\Delta t = 0.02$ s and $\Omega = 0$ rad/s.

In Fig. 1, the time evolution of the kinetic energy K is shown. The cases with $\Delta t = 0.02$ and 0.015 s calculated by the standard algorithm are blown up and cannot give stable results. The cases with $\Delta t = 0.01$, 0.005 and 0.00002 s calculated by the standard algorithm are stable. The stability analysis in Section 2.3 shows that the stability condition of RK4 for the Coriolis term is $\Delta t \leqslant 1.415/\Omega = 0.01415$ s, and the numerical results support the analysis. However, the solution of the case with $\Delta t = 0.01$ s is very different from the converged solution (i.e. the case with $\Delta t = 0.0002$ s). This difference is considered due to the influence of the diffusion error of RK4. Hence, to obtain a reliable solution of a strong rotation case with an explicit scheme, the time increment should be set very small, on the order of 10^{-4} in this case. On the other hand, with the present algorithm proposed in Section 3.2, even the cases with $\Delta t = 0.01$ and 0.02 s can give almost the same solution as that with $\Delta t = 0.0002$ s using the standard algorithm. There is no diffusion error regarding the Coriolis term in the results with the present algorithm. In the present study, we also confirmed that, when the stability condition for the nonlinear term is satisfied, i.e. the Courant number does not exceed a critical value, the present algorithm is always stable, no matter how strong the rotation is. The verification shows that the present algorithm is useful for DNS of strong rotating flow and saving total computational costs.

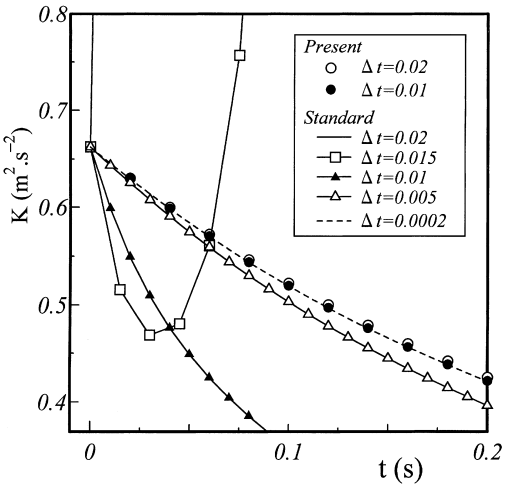

Fig. 1. Evolution of kinetic energy in a verifying simulation (Δt (s)).

4. DNS of rotating decaying turbulence

4.1. Initial conditions

We apply the present algorithm to DNS of the initially isotropic decaying turbulence with or without system rotation. The computational region is the same as that of the verifying simulation. The spectral mode number is 96 in each direction. The time increment and the kinetic viscosity are 0.01 s and 0.005 m/s, respectively. In this study, first, a velocity field with random phase in the Fourier space is produced with the following energy spectrum profile (Squires et al., 1994):

$$E(k,0) = \left(\frac{2048}{9\pi}\right)^{1/2} q_0 \frac{k^4}{k_\mathrm{p}^5}\exp\left(-\frac{2k^2}{k_\mathrm{p}^2}\right), \tag{15}$$

where $q_0 = 1.5$, $k_\mathrm{p} = 5$ are used. A nonrotating pre-computation is started with this spectrum and run up to a time $t_0 = 1.0$ s to obtain a value near -0.5 for the velocity gradient skewness (Orszag and Patterson, 1972) and a reliable power-law for the turbulent kinetic energy. This pre-computation is important for the field to build the correlations. Then the system rotation is introduced into the flow field at t_0 as an initial condition for this study. Without loss of generality, we set the x_3-axis as the rotation axis. DNS with $\Omega = 0$, 1, 2, 5, 10, 20, and 100 rad/s ($\Omega k_0/\varepsilon_0 = 0$, 0.983, 1.96, 4.92, 9.83, 19.6 and 98.3) are carried out to investigate the effects of the system rotation on turbulence. Table 2 presents the properties of the initial turbulent field.

4.2. Results and discussion

Fig. 2 shows the evolution of the turbulence kinetic energy K. As demonstrated theoretically by Cambon et al. (1997) and Mansour et al. (1992), the decay of kinetic energy is inhibited

Table 2
Parameters of the initial field (at $t = t_0$)

K_0 (m^2 s^{-2})	ε_0 [m^2 s^{-3}]	Re_t	Re_λ	S	F
0.7023	0.7147	138.01	23.496	−0.485	4.057

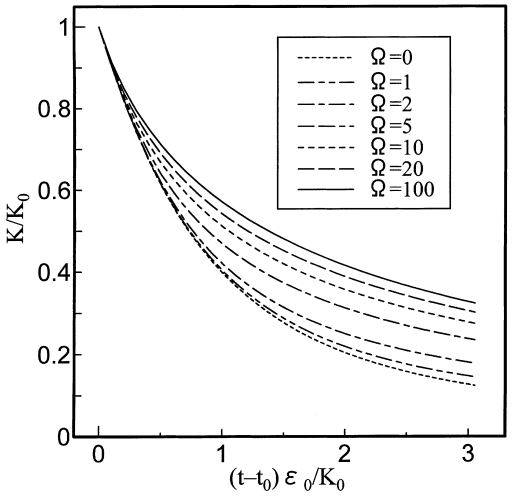

Fig. 2. Evolution of kinetic energy (Ω (rad s^{-1})).

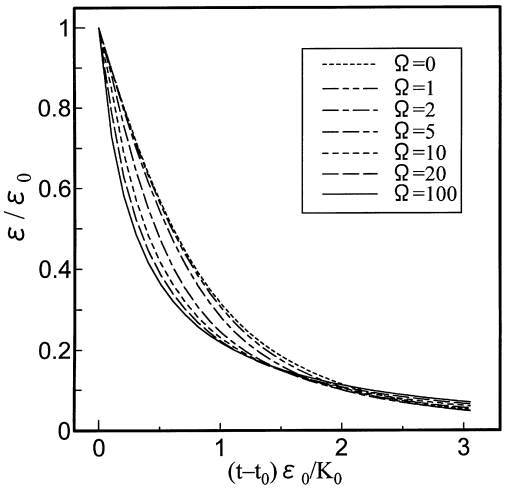

Fig. 3. Evolution of energy dissipation rate (Ω (rad s^{-1})).

by the system rotation. Considering the budget of the kinetic energy, that is $dK/dt = -\varepsilon$, one can predict the influence of the rotation on the dissipation rate. In Fig. 3, the evolution of the dissipation rate ε is presented. The system rotation accelerates the decay of the dissipation rate in the initial period. It can be considered the very reason why the system rotation inhibits the decay of kinetic energy. For more details about the effect, we investigated the budget of the dissipation rate in Fig. 4. The budget equation reads

$$\frac{d\varepsilon}{dt} = P_\varepsilon - D_\varepsilon, \tag{16}$$

where P_ε and D_ε are the production and the destruction terms of ε, respectively,

$$P_\varepsilon = -2\nu\overline{\frac{\partial u_i}{\partial x_j}\frac{\partial u_i}{\partial x_l}\frac{\partial u_j}{\partial x_l}}, \quad D_\varepsilon = 2\nu^2\overline{\frac{\partial^2 u_i}{\partial x_j \partial x_l}\frac{\partial^2 u_i}{\partial x_j \partial x_l}}.$$

As shown in Fig. 4, the production and the destruction terms are decreased simultaneously by the rotation. But the rotation affects the production term more strongly than the destruction term. In particular, in the case with $\Omega = 100$ rad/s, the value of P_ε decreases to almost zero instantly, while the value of D_ε decreases more slowly. The system rotation promotes the decay of the dissipation rate in the initial period of evolution. However, P_ε and D_ε of cases with strong rotation tend to zero faster than those with weak or no rotation. This is why the dissipation rate with strong rotation is larger than that with weak rotation in the later period of the evolution, as shown in Fig. 3.

The effect of rotation on turbulence can be exhibited in wave space too. The evolution equation of the energy spectrum $E(k,t)$ is

$$\left(\frac{\partial}{\partial t} + 2\nu k^2\right)E(k,t) = T(k,t). \tag{17}$$

Here $T(k,t)$ corresponds to the triple-velocity correlations coming from the nonlinear interactions of the N–S equations, and it is called the energy transfer function. The profile of the energy transfer function at $t - t_0 = 1$ s is shown in Fig. 5. With an increase of the rotation from 0 to 100 rad/s, the absolute value of $T(k,t)$ decreases gradually. Accordingly, the energy transfer from low to high wave number is decreased by the system rotation. In other words, the energy cascade is inhibited by the system rotation. Theoretical analysis (Kassinos and Reynolds 1994; Cambon et al., 1997) demonstrated that the nonlinear interactions could be ignored, i.e. $T(k,t) \cong 0$, when the rotation is strong enough. This simplification yields a linear solution directly from Eq. (17),

$$E(k,t) = E(k,0)\exp(-2\nu k^2 t). \tag{18}$$

Fig. 6 shows the variation in the turbulence energy spectrum with the rotation rate Ω. The system rotation inhibits the kinetic energy cascade from the lower to the higher wave number. Fig. 6 also shows that after the same time evolution, the energy of a strong rotation case is larger than that of a weak or no rotation case in the low wave number region of the spectrum, and vice versa in the high wave number region. In addition, the energy spectrum profile of the case with $\Omega = 100$ rad/s fits very well with the linear solution of Eq. (18) in the low wave number region. Considering that most of the spectral energy concentrates in the low wave number region, the simplification above appears reasonable for strong rotation.

Rotation also affects the turbulence velocity distribution and the structure in wave space. Figs. 7 and 8 show the distribution of the real part of the velocity on a 1/8 shell of radius $k = 5$ and 30, respectively, in the wave space. Figs. 7(a) and 8(a) present the initial distribution of the velocity. The orientations of velocity vectors are distributed randomly on the tangent plane of the shell due to the solenoidal condition. The moduli of these vectors have almost the same order. When the system is not subjected to rotation (Figs. 7(b) and 8(b)), the

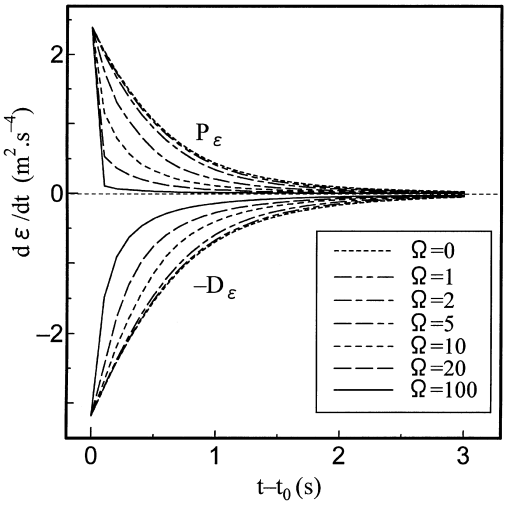

Fig. 4. Budget of energy dissipation rate (Ω (rad s^{-1})).

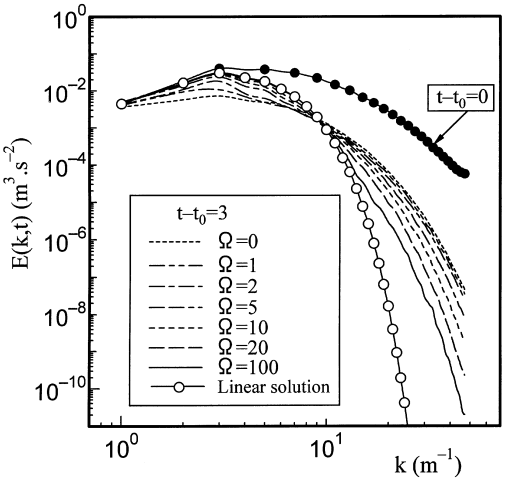

Fig. 6. Profile of energy spectrum at $t - t_0 = 3$ s (Ω (rad s^{-1})).

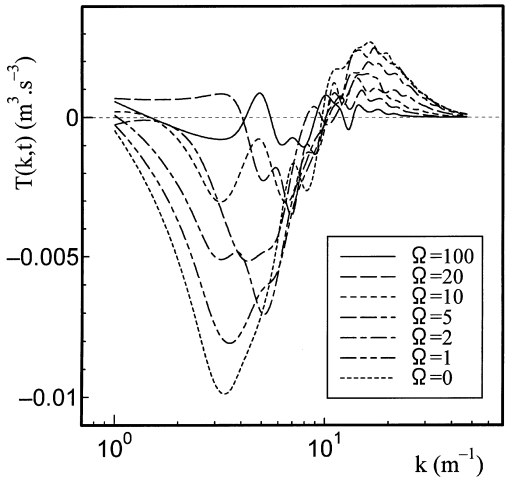

Fig. 5. Profile of energy transfer function at $t - t_0 = 1$ s (Ω (rad s^{-1})).

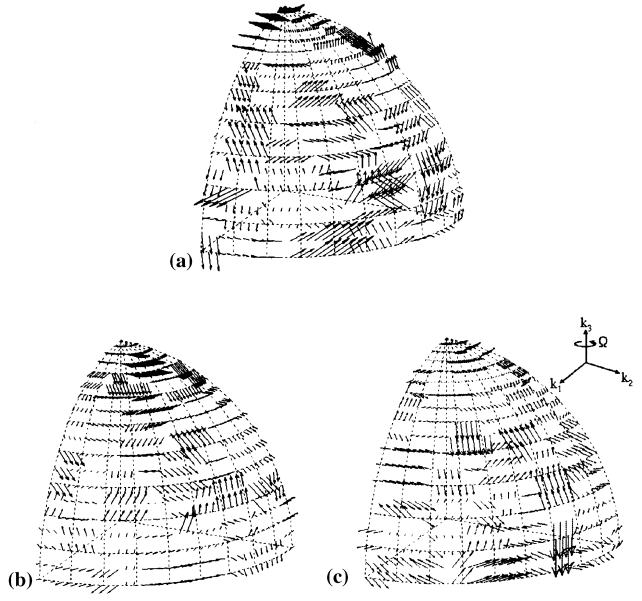

Fig. 7. Distribution of the velocity coefficient (real part) on the shell of radius $k = 5$: (a) $t - t_0 = 0$ s; (b) $\Omega = 0$ rad s^{-1}, $t - t_0 = 1$ s; (c) $\Omega = 10$ rad s^{-1}, $t - t_0 = 1$ s.

distribution does not present any apparent change with time, while the moduli of these vectors decrease due to the viscous effect. However, the distribution of the velocity vectors of the rotating case (Figs. 7(c) and 8(c)) is very different from that of a case with no rotation. Besides the viscous effect, the moduli of the vectors decrease gradually from the equator to the pole. In particular, in the case of $k = 30$, vectors near the pole have almost zero moduli, indicating that the local decay of energy near the pole is faster than that of the equator. Therefore, an anisotropic distribution of the kinetic energy between the pole and the equator is presented in wave space. Considering that the energy transfer is inhibited by the system rotation, the energy of the rotating system is lower than that of the non-rotating system in the low wave number region and vice versa in the high wave number region. In accordance with these results, in the low wave number region, the moduli of the vectors of a rotating case (Fig. 7(c)) at the equator are larger than those of a nonrotating case (Fig. 7(b)). It can be considered that the energy in a rotating system is transferred locally from the pole to the equator, i.e. the energy is concentrated in the plane near the equator. On the other hand, in the high wave number region, even on the equator plane, the moduli of the vectors of a rotating case (Fig. 8(c)) are smaller than those of a nonrotating one (Fig. 8(b)).

Fig. 9 shows the iso-surface of the absolute value of the vorticity within the computational box. The value for the iso-surface is set as double of r.m.s. vorticity. There exist fine and isotropically distributed vortex structures initially (Fig. 9(a)). The vorticity is stretched by the turbulence and the system rotation, and large and elongated structures appear along the axis of rotation (Fig. 9(c)), while the vorticity is only stretched by the turbulence and exhibits a homogeneous distribution in a nonrotating system (Fig. 9(b)). This phenomenon is the so-called two-dimensionalization, which can be presumably explained by the classic Proudman–Taylor theorem. But Cambon et al. (1997) argued that the transition from a three-

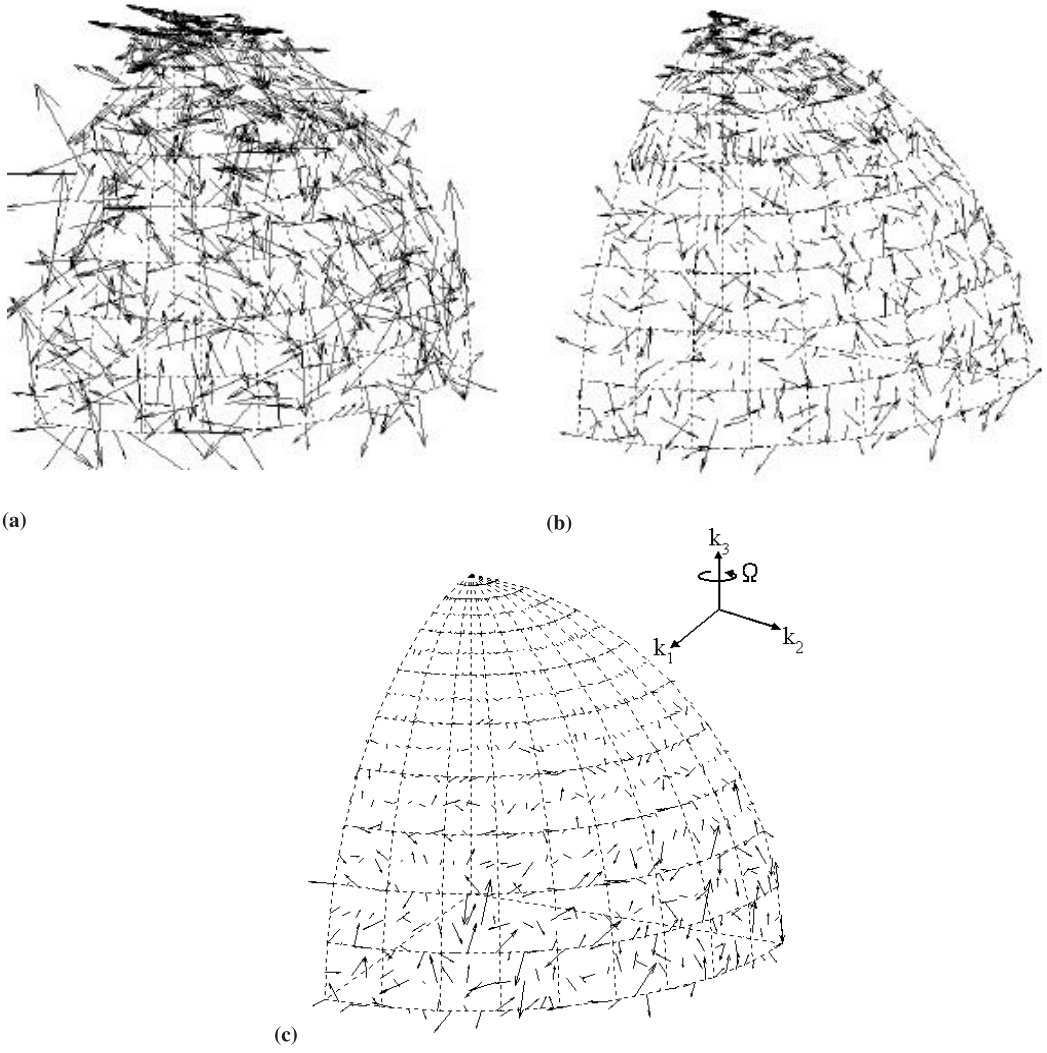

Fig. 8. Distribution of the velocity coefficient (real part) on the shell of radius $k = 30$: (a) $t - t_0 = 0$ s; (b) $\Omega = 0$ rad.s^{-1}, $t - t_0 = 1$ s; (c) $\Omega = 10$ rad s^{-1}, $t - t_0 = 1$ s.

dimensional to a two-dimensional structure is linked to both the nonlinear interactions and the system rotation. Too weak rotation cannot affect the dynamics of three-dimensional isotropic turbulence, and too strong rotation deduces a pure viscous decaying turbulence while the nonlinear interactions are damped through the scrambling effect. Therefore, a direct deduction from their argument is that only a moderate rotation can influence the transition obviously. Fig. 10 shows the two-dimensionalization phenomenon quantitatively. In Fig. 10, the evolution of the ratio L^* of the transverse integral lengthscale to the longitudinal one is presented. The integral lengthscale is given by

$$L_{ij,k} = \int_0^\infty \langle u_i(x) u_j(x + r\boldsymbol{n}^k) \rangle \mathrm{d}r / \langle u_i(x) u_j(x) \rangle. \tag{19}$$

From Fig. 10, the cases with the moderate rotation ($\Omega = 5, 10$ rad/s or $Ro^L = 0.273, 0.137$) indicate faster development of L^*, which means that the development of the transverse integral lengthscale is faster than that of the longitudinal one. On the other hand, the weakest rotation ($\Omega = 1$ rad/s or $Ro^L = 1.37$) and the strongest rotation ($\Omega = 100$ rad/s or $Ro^L = 0.0137$) increase L^* more slowly than the moderate rotation. This confirms the argument of Cambon et al. (1997).

5. Conclusions

The numerical stability of a number of time marching methods for the governing equations of rotating flow has been discussed. Explicit methods with an accuracy not lower than thirdorder should be applied in order to simulate the NS equations with the Coriolis term stably. Solving the Coriolis term by an explicit method introduces a diffusion error into the solution. In this paper, a new DNS algorithm has been proposed for rotating turbulence. In this algorithm the Coriolis term is integrated analytically, based on the diagonal governing equations and the integral factor technique. The verification shows that the algorithm proposed in this paper is stable in simulating the strong rotating turbulence and saves total computational costs.

Then, the new algorithm is applied to DNS of the rotating turbulence to investigate the effects of rotation on the statistics and the vortical structure of the turbulence. The DNS results show that the main influences of the system rotation on the

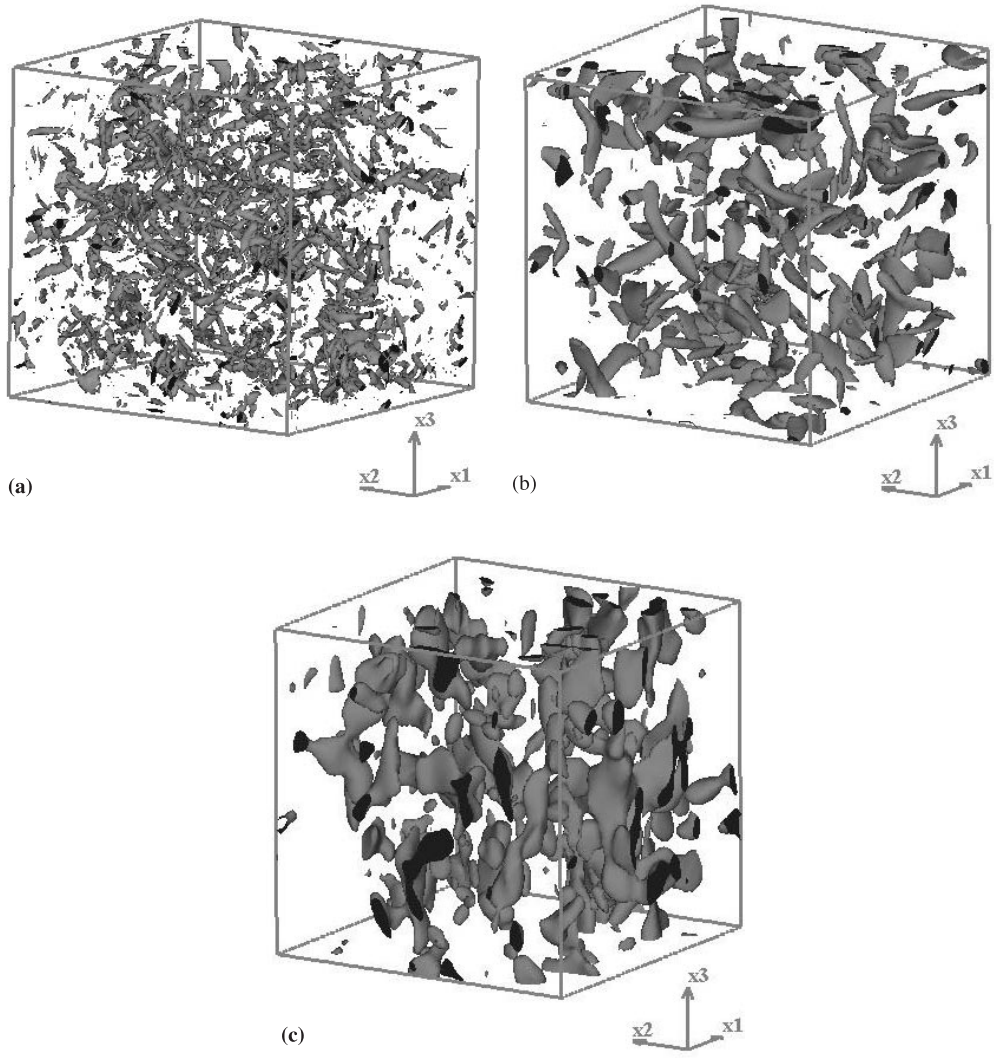

Fig. 9. Iso-surface of the absolute value of the vorticity: (a) $t - t_0 = 0$ s; (b) $\Omega = 0$ rad s^{-1}, $t - t_0 = 6$ s; (c) $\Omega = 10$ rad s^{-1}, $t - t_0 = 6$ s.

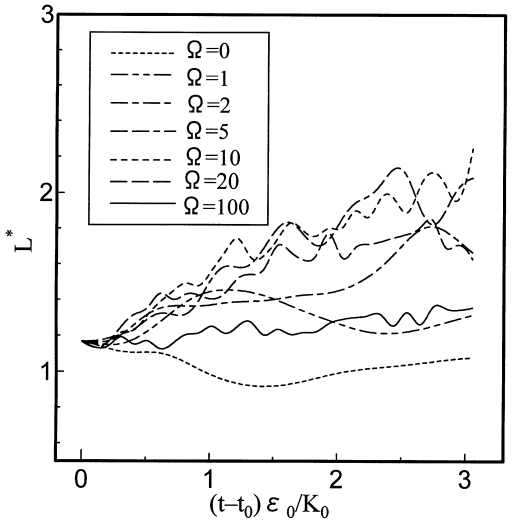

Fig. 10. Evolution of integral lengthscale (Ω rad s^{-1}).

turbulence are twofold. One is that rotation inhibits the decay of the kinetic energy. Although the system rotation reduces both the production and the destruction terms of the evolution equation of the dissipation rate, the production term decreases faster to zero than the destruction term. Then the total effect of the system rotation is to accelerate the decrease of the dissipation rate, which directly leads to the inhibition of kinetic energy decay. With a very strong rotation, the decaying behavior of the turbulence tends to that of the pure linear system. The other effect of the system rotation is two-dimensionalization. That is, rotation deduces an anisotropic distribution of the kinetic energy between the pole and the equator in wave space, and elongates the vortical structure along the rotational axis in physical space. This rotation effect is only apparent at moderate rotation. Both at weak and strong rotations, the transition from the three-dimensional to the two-dimensional structure due to the combined effect of the nonlinear interactions and the system rotation is difficult to obtain.

References

Bech, K.H., Tillmark, N., Andersson, H.I., 1995. An investigation of turbulent plane Couette flow at low Reynolds numbers. J. Fluid Mech. 286, 291–325.

Cambon, C., Jacquin, L., 1989. Spectral approach to non-isotropic turbulence subjected to rotation. J. Fluid Mech. 202, 295–317.

Cambon, C., Mansour, N.N., Godeferd, F.S., 1997. Energy transfer in rotating turbulence. J. Fluid Mech. 337, 303–332.

Canuto, C., Hussiaini, M.Y., Quarteroni, A., Zang, T.A. (Ed.), 1987. Spectral Methods in Fluid Dynamics. Springer, Berlin, pp. 203–212.

Gear, C.W., 1971. Numerical Initial Value Problems in Ordinary Differential Equations. Prentice-Hall, Englewood Cliffs, NJ, pp. 25–44, 102–135.

Hossain, M., 1994. Reduction in the dimensionality of turbulence due to a strong rotation. Phys. Fluids A 6 (3), 1077–1080.

Jacquin, L., Leuchter, O., Cambon, C., Mathieu, J., 1990. Homogeneous turbulence in the presence of rotation. J. Fluid Mech. 220, 1–52.

Kassinos, S.C., Reynolds, W.C., 1994. A structure-based model for the rapid distortion of homogeneous turbulence. Technical Report TF-61, Stanford University, pp. 373–387.

Kristoffersen, R., Anderson, H.I., 1993. Direct simulations of low-Reynolds number turbulent flow in a rotating channel. J. Fluid Mech. 256, 163–197.

Lamballais, E., Lesieur, M., Metais, O., 1996. Effects of spanwise rotation on the vorticity stretching in transitional and turbulent channel flow. Int. J. Heat Fluid Flow 17, 324–332.

Lesieur, M., 1997. Turbulence in Fluids (third revised and enlarged ed.). Kluwer Academic Publishers, The Netherlands, 143–146.

Mansour, N.N., Cambon, C., Speziale, C.G., 1992. Single point modeling of initially isotropic turbulence under uniform rotation. Center for Turbulence Research Annual Research Briefs-1991, Stanford Univ./NASA Ames., pp. 159–167.

Moin, P., Mahesh, K., 1998. Direct numerical simulation: a tool in turbulence research. Annu. Rev. Fluid Mech. 30, 539–578.

Orszag, S.A., Patterson, G.S., 1972. Numerical simulations of turbulence. In: Rosenblatt, M., Van Atta, C. (Eds.), Statistical Models and Turbulence, vol. 12. Springer, Berlin, pp. 127–147.

Rogallo, R.S., 1981. Numerical experiments in homogeneous turbulence. NASA Tech. Memo TM81315, pp. 1–91.

Smith, L.M., Waleffe, F., 1999. Transfer of energy to two-dimensional large scales in forced, rotating three-dimensional turbulence. Phys. Fluids A 11 (6), 1608–1622.

Squires, K.D., Chasnov, J.R., Mansour, N.N., Cambon, C., 1994. Investigation of the asymptotic state of rotating turbulence using large-eddy simulation. Center for Turbulence Research Annual Research Briefs-1993, Stanford Univ./NASA Ames., pp. 157–170.

Tafti, D.K., Vanka, S.P., 1991. A numerical study of the effects of spanwise rotation on turbulent channel flow. Phys. Fluids A 3 (4), 642–656.

Teissedre, C., Dang, K., 1987. Anisotropic behavior of rotating homogeneous turbulence by numerical simulation. AIAA paper 87–1250, pp. 1–7.

Waleffe, F., 1992. The nature of triad interactions in homogeneous turbulence. Phys. Fluids A 4 (2), 350–363.

Yang, K.S., Kim, J., 1991. Numerical investigation of instability and transition in rotating Poiseuille flow. Phys. Fluids A 3 (4), 633–641.

Yeung, P.K, Zhou, Y., 1998. Numerical study of rotating turbulence with external forcing. Phys. Fluids A 10 (11), 2895–2909.